A Catalyst free - green synthesis of novel benzylindenoquinoxaline compounds containing 1,2-diketone moiety: geometrical, electronic structural studies and biological activities.

Venkadachalam Rahimiya[a], Mahesh Kalidasan[b], Krishnamoorthy Bellie Sundaram[c] and Appaswami Lalitha [a*]

[a]Department of Chemistry, Periyar University, Salem-636011, Tamil Nadu, India.

[b]Department of Chemistry, Mahendra Arts & Science College, Namakkal-637501.

[c]Department of Chemistry (SF), PSG College of Arts and Science, Coimbatore, Tamil Nadu, India-641014.

*Corresponding author e-mail: (AL) lalitha2531@yahoo.co.in, lalitha253@periyaruniversity.ac.in; Tel: +91-427-234-5271; Fax: +91-427-234-5124;

Abstract:

Benzoyl indenoquinoxalines (BIQ) were synthesized by the cyclocondensation method of 3,4-diaminobenzophenone with 1,2-diketone derivatives in the presence of ethanol at room temperature. The reaction protocol is very simple that avoids toxic solvents and catalysts, resulting in a more environmental friendly synthetic method. Using this method, quinoxaline derivatives as biologically potent molecules are formed with excellent yields in shorter reaction times. Benzyl indenoqunioxalines synthesized were characterized by using FT-IR, NMR, and Mass spectral studies. The molecular structures of two selected benzyl indenoqunioxalines were also confirmed by the single crystal X-ray diffraction method. Moreover, molecular docking studies of these compounds showed more effective binding with human epidermal growth factor receptor tyrosine kinase (4HJO). Theoretical calculations at the DFT (BP86/Def2-TZVP) level supported the experimental findings. The reactivity of the quinoxaline compounds was examined using the global reactivity descriptors and the frontier molecules orbitals (FMOs). The antimicrobial activities of the synthesized quinoxaline compounds against bacterial species such as *Staphylococcus aureus, Escherichia coli* and *Klebsiella pneumoniae* in different concentrations reveal notable responses depending on the strain and the concentration of the compounds examined.

Graphical Abstract

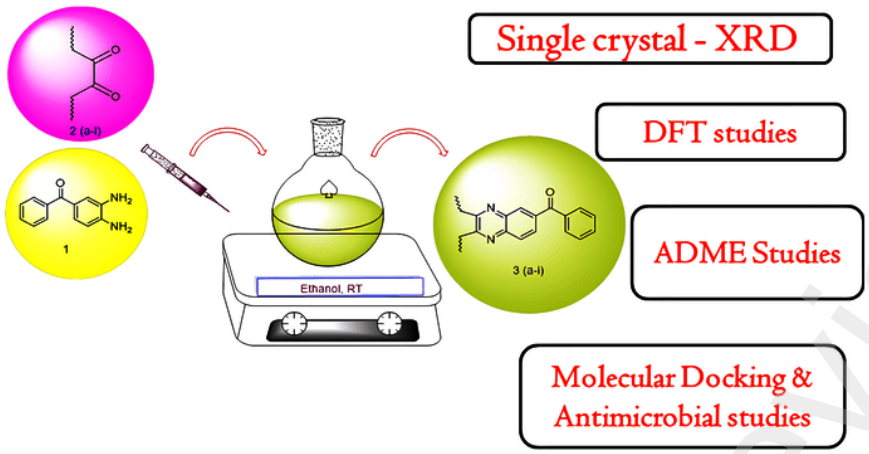

***Keywords*:** Benzyl indenoquinoxaline derivatives; Single crystal-XRD, Antibacterial activity; Density functional theory; Molecular docking.

1. Introduction

Heterocyclic compounds, especially the nitrogen containing heterocycles have a wide-ranging of applications, in the fields of pharmaceutical [1-4], agrochemicals, and natural products [5]. Quinoxalines, a class of N-heterocyclic compounds, have important biological applications, and industrial quinoxaline (C=N) compounds are the most important because, they are the backbone of a large variety of products such as intermediates for the preparation of new biologically active substances and also used in marketed drugs [6-7]. Owing to their excellent bioactivity, quinoxaline motifs remain the backbone of many fungicides, herbicides, and insecticides, and pharmaceutically important anticancer, anti-inflammatory, anticancer, antibacterial, antiviral, and antimalarial drugs [8-11]. In the research towards the expansion of efficient and environmentally benign synthetic methodologies, use of eco-friendly conditions such as catalyst free, cost efficiency, experimental ease, easy work-up, and simple recovery have become attractive in the recent chemistry world [14].

Among various quinoxaline derivatives, indenoquinoxaline derivatives exhibit a wide range of biological actions, including antimycobacterial [15], antibacterial, antifungal, antiviral [16], anticancer [17], antiprotozoal, and antipasmodial effects [18-20]. Additionally, indeno[1,2-b]quinoxalines have been proved as potential acid corrosion inhibitors for mild steel surfaces [21], utilized in electrical-photochemical materials, dyes, organic semiconductor production, anion receptors, and synthesis of dehydroannulenes, electroluminescent materials and DNA-cleaving agents [22, 23].

Recently, Y. Li and colleagues reported the synthesis of (2,3-bis(4-(dimethylamino)phenyl)quinoxalin-6-yl)(phenyl)methanone by the reaction of 3,4–diaminobenzophenone with benzil using acetic acid under the reflux conditions [24]. S. Sajjadifar et al., reported the synthesis of 9-methylacenaphtho [1,2-b]quinoxaline via one pot two component reactions of 3,4-diaminobenzophenone and acenaphthoquinone using phthalic acid as a catalyst at room temperature [25]. Y. Kaya and co-workers reported the

synthesis of 7-benzoyl quinoxaline from 3,4-diaminobenzophenone and glyoxal using methanol as a solvent [26]. A. Mishra and co-workers synthesized 11*H*-indeno[1,2-b]quinoxalin-11-one via ultra-sonication method from *o*-phenylenediamine and ninhydrin using water as a solvent [27]. D. N. Kanekar and his groups reported the synthesis of indolo[2,3-b]quinoxalin-2-yl(phenyl)methanone from 3,4-diaminobenzophenone and 5-substituted-1-methyl-1*H*-indole-2,3-dione using acetic acid under the reflux conditions [28]. The energy and quantum chemical calculations have been derived using DFT, ADME and similar *in-silico* studies that well supported the experimental results [29].

In the present work, the synthesis of 8-benzoyl-11*H*-indeno[1,2-b]quinoxaline-11-one derivatives in ethanol through a one-pot two component reaction of 3, 4-diaminobenzophenone (DABP) with different 1,2-dicarbonyl compounds (ninhydrin, isatin, benzil, 2-hydroxynapthoquinone, alloxan or oxalic acid) leading to novel 8-benzoyl-11*H*-indeno[1,2-b]quinoxaline-11-one derivatives under greener conditions has been described. From the literature review, it is evident that most of the published research in this area have limitations such as extended reaction times, complex purification processes, use of many hazardous solvents such as THF, methanol and catalysts such ethylene glycol, acetic acid and H_2SO_4, and low yields. The present work aimed to improve the yields (98%), under catalyst free and greener solvent conditions which lead to eco-friendlier reactions.

Spectroscopic analyses were used to characterize the synthesised substances. Additionally, single crystal X-ray diffraction examinations were used to confirm the molecular structures of two chosen compounds. Computational chemistry tools like DFT methods are successfully used in the mechanistic investigation, to help the complete characterization of the synthesized molecules and also to investigate the molecular orbital interactions [30-36]. The DFT methods helped to study the molecular structure and reactivity descriptors of the benzyl indenoquinoxaline compounds through electronic structural analysis. In addition, the molecular properties of the optimized structure were defined by computational studies. Molecular docking studies of these compounds showed dynamic

binding with human epidermal growth factor receptor tyrosine kinase (4HJO). The newly developed compounds were compared with the traditional antibiotic, *streptomycin*. The *in-vitro* antibacterial activity studies of the synthesized compounds against highly pathogenic bacteria like *Streptococcus aureus*, *Klebsiella pneumoniae* and *Escherichia coli* under similar conditions revealed that the benzyl indenoquinoxaline may be considered as an excellent starting molecule for the synthesis of new bioactive compounds.

2. Experimental Section

2.1. Physical methods and materials

All of the reagents used in this work were obtained commercially and used precisely as directed. Ninhydrin, alloxan, oxalic acid, benzil, acenaphthoquinone were acquired through Sigma Aldrich (Bengaluru, India), 3,4-diaminobenzophenone, isatin derivatives were purchased from Loba Chemie (Hyderabad, India) and used without further any purification. The solvents were purified according to standard procedures [37]. All the reactions were carried out at ambient temperature. TLC analysis of all reactions were performed on Merck precoated plates (silica gel 60F-254), and analysed by either placing it in an iodine chamber or under intense UV illumination. Melting points were determined using an electrothermal 9200 device with the capillary tube method and are uncorrected. IR spectra were recorded a Perkin Elmer FT-IR spectrometer with scanning between 400-4000 cm^{-1}. NMR spectra were obtained a Bruker DRX-400MHz NMR instrument in DMSO-D_6 solvent with TMS as an internal standard. High-resolution mass spectra of representative compounds were recorded with the maXis 10138 mass spectrometer operating at 70 eV.

2.2. General procedure of synthesis of quinoxaline derivatives

Benzyl indenoquinoxaline derivatives were synthesized by simple cyclocondensation between 3,4- diaminobenzophenone and 1,2-diketone moieties. Equimolar solutions of 3,4–diaminobenzophenone (**1**) with 1,2 diketones such as ninhydrin (**2a**), isatin (**2b**), 5-nitro-isatin (**2c**), 5-chloroisatin (**2d**), acenaphoquinone (**2e**), benzil (**2f**), 2-hydroxynapthoquinone

(**2g**), alloxan (**2h**), or oxalic acid (**2i**) in 10 ml ethanol was stirred without catalyst at room temperature to obtain the corresponding benzylindenoquinoxaline compounds (**3a-i**). The progress of the reaction was monitored by TLC (ethylacetate: *n*-hexane, 7:3). Then the precipitate was filtered and washed with water and ethanol in order to obtain the pure product. A Single crystal XRD study was obtained by recrystallization of these crystals in ethyl acetate/THF mixture.

2.3. X-ray structure analyses

Fluorescent orange crystal (**3a**) and brown crystal (**3f**) were obtained in THF /Ethyl acetate solutions of corresponding compounds by the slow evaporation method. Single crystal - XRD data parameters were carried out on a Bruker D8 Quest Eco diffractometer. Crystal data were collected at 296K using graphite-monochromatic MoKα radiation (λα = 0.7107 Å). The plan for the data collection was calculated using the structure that was solved and refined using the Bruker SHELXTL Software Package. The molecular structures were solved by direct method using the program SHELXS-2019 and refinement done by full-matrix least square methods with SHELXL-2019 refined on F^2 [38, 39]. Direct methods were used to determine the positions of every atom. All non-hydrogen atoms underwent anisotropic refinement. With isotopic temperature factors that are typically 1.2Ueq of their parent atoms, the hydrogen atoms were arranged in geometrically restricted places.

2.4. Computational details

2.4.1. Theory

Molecular properties like chemical hardness (η), electronegativity (χ), electrophilicity (ω), ionization potential (A) and electron affinity (I) have been defined based on the DFT method [40-43]. The value of chemical hardness may give an idea on the chemical stability and reactivity of a molecule [44]. Electronegativity (χ), and Chemical hardness (η), were defined as follows [45]:

$$\text{Chemical Hardness } (\eta) = \frac{1}{2}\left[\frac{\partial^2 E}{\partial N^2}\right]_{V(r)}$$

$$\text{Electronegativity } (\chi) = \frac{1}{2}\left[\frac{\partial E}{\partial N}\right]_{V(r)}$$

where V(r) and E are external potential and electronic energy of system in N number of electron respectively. For closed-shell molecules, Koopman's theorem enables us to define η and χ as

$$I = -\varepsilon_{\text{HOMO}},\ A = -\varepsilon_{\text{LUMO}}$$

$$\eta = \frac{I - A}{2}$$

$$\chi = \frac{I + A}{2}$$

where I and A stand for the ionization potential and electron affinity. While electron affinity describes a ligand's ability to take exactly one electron from a donor, ionization potential describes a molecule's susceptibility to loose an elctron. Electrophilicity (ω) can be defined as a decrease in energy caused by the maximum electron flow between the donor and the acceptor [46]. It can be described as:

$$\omega = \frac{\chi^2}{2\eta}$$

The $E_{\text{LUMO-HOMO}}$ energy gap also included in this study as a quantum mechanical descriptor. The HOMO-LUMO energy gap can be efficiently used in establishing a relationship between the chemical structure of compounds and their biological activity [47-49].

2.4.2. DFT Studies

The DFT calculations were performed with the ORAC software developed by Frank Neese and co-workers [50]. All calculations were carried out using BP86 density functional [51-53] and Def2-TZVP basis set included in the ORCA program, which is free for academic use. The TIGHTSCF convergence criteria has been used while performing the self-consistent field (SCF) calculations. The DFT optimized geometries were confirmed as minima in the

potential energy surface. The graphics program ChemCraft has been successfully used for getting the pictures of the optimized geometries and the frontier molecular orbitals [54].

2.5. Molecular Docking Studies

For the docking analysis, BIQ was chosen and subjected to optimization and minimization using LigPrep with the OPLS3 force field. The crystal structure of EGFR tyrosine kinase with (Protein data bank ID: 4HJO) was attained from the Protein Data Bank [55]. During the preparation process, prescribed bond orders were consigned, and water molecules were removed. The protein structure was completed by adding hydrogen atoms, charges, and any side chains that were missing from any residues. The prepared structures were then optimized and minimized to resolve any steric clashes, utilizing the OPLS3 force field and the preparation of protein occurrence in Schrödinger's Maestro 8.0 software. Following the standard protocol, a grid box was centered on the binding site, identified through site map analysis [56]. The ligands were then docked using the Glide module, which performs flexible ligand docking to find the best fit within the binding site. The resultant protein ligand complex structure was determined using Biovia discovery studio [57].

2.6. ADME analyses

The Swiss ADME free web server of online tool (http://swissadme.ch/index.php), has been used to get the synthetic accessiblity, bioavailability score, and several pharmacokinetic parameters of the benzyl indenoquinoxaline derivatives (3h-3i) and the maximum active and positive control were determined [58, 59]. Accordingly, for all the synthesized compounds, the calculations were performed using Swiss ADME software and the results are shown in Table 11-13.

2.7. Antibacterial study

To evaluate the antibacterial properties of the synthesized compounds, uncultured pathogens such as Stapylococcus sp. MG87 (2013) (NCBI-Accession: KC68883.1) and Klebsiella sp. clone MASC-TSK (NCBI-Accession: KF649832.1) were clinically isolated. We purchased standard E. Coli strains (MTCC-443) from MTCC Chandigarh, India. According to the protocol described in the literature, the newly synthesized benzyl indenoquinoxaline derivatives 3(a-i) were dissolved in dimethylsulfoxide (DMSO) at a concentration of 25 μg ml^{-1} and tested using the agar well diffusion method against human pathogenic bacteria of Gram negative strain viz., *(i) Klebsiella pneumonia* (MTCC 424) (ii) *Escherichia coli* (MTCC 443), and Gram positive strain (iii) *Staphylococcus aureus* (MTCC 96) [60, 61]. The three bacteria exponentially developing cultures in nutrient broth at 37°C were diluted in sterile broth after 18 hours. The agar diffusion technique was employed to ascertain the initial screening of antibacterial efficacy. The average diameter of the bacterial growth inhibition zone (IZ) surrounding the disc was measured for each tested drug and disc in mm (Table-14). Dimethylsulfoxide solvent served as the negative control, and streptomycin as the positive control. All the samples were taken in triplicates.

2.8. Spectral details for synthesis of benzyl indenoquinoxaline derivatives

2.8.1. 8-Benzoyl -11H-indeno[1,2-b]quinoxaline-11-one (3a)

Yield: 99%; Colour: Yellow solid; M.P: 289°C;FT-IR (KBr): 3063(CH Str), 1726 (C=O Str), 1654 (C=N Str), 1576, 1487, 1335, 1191, 766, 719 cm^{-1}; ^{1}H NMR (400 MHz, DMSO-D_6): δ 8.54 (d, 1H CH), 8.28 (dd, 1H CH), 8.17 (d, 1H CH), 8.09 (d, 1H CH), 7.89 (m, 3H CH), 7.78 (t, 1H CH), 7.64 (m, 2H CH), 7.53 (t, 2H CH); ^{13}C NMR (400 MHz, DMSO-D_6) δ 194.87, 189.09, 157.97, 150.20, 144.97, 141.63, 141.05, 138.34, 137.04, 136.88, 136.68, 136.69, 134.26, 133.17, 133.06, 132.36, 128.18, 124.88, 122.94; MALDI-TOF: m/z calcd for $C_{22}H_{12}N_2O_2$ 336.08 (M^+), found 338.07.

2.8.2. 9-Benzoylbenzo[4,5]imidazo[1,2-c]quinazolin-6(5H)-one (3b)

Yield: 67%; Colour: Orange solid; M.P:293°C; FT-IR (KBr): 3384 (NH Str), 2922, 2851, 1649 (C=O Str), 1609 (C=N Str), 1564, 1361,1214,1118, 872, 716cm^{-1}; ^{1}H NMR (400 MHz, DMSO-D_6): δ 12.53 (s, 1NH), 8.23 (dd, 1H CH), 7.95 (d, 1H CH), 7.79 (dd, 2H CH), 7.72 (m, 2H CH), 7.63 (m, 3H CH), 7.17 (m, 1H CH), 6.83 (dd, 1H CH), 6.59 (m, 1H CH); ^{13}C NMR (400 MHz, DMSO-D_6) δ 195.37, 158.28, 155.16, 149.81, 137.37, 137.23, 134.19, 133.35, 132.13, 131.88, 131.65, 130.14, 129.12, 128.50, 124.50, 117.13, 116.82, 114.92; MALDI-TOF: m/z calcd for $C_{21}H_{13}N_3O_2$ 339.10 (M^+), found 340.18.

2.8.3. 9-Benzoyl-2-nitrobenzo[4,5]imidazo[1,2-c]quinazolin-6(5H)-one (3c)

Yield: 75%; Colour: Yellow solid; M.P: 301°C; Yellow solid; FT-IR (KBr): 3345 (NH Str), 2918, 1668 (C=O Str), 1644 (C=N Str), 1593, 1575, 1281, 581cm^{-1}; ^{1}H NMR (400 MHz, DMSO-D_6): δ 12.73 (s, 1H NH), 8.70 (d, 2H CH), 8.53 (d 2H CH), 8.05 (dd 2H CH), 7.58 (dd, 2H CH), 7.30 (d, 3H CH); ^{13}C NMR (400 MHz, DMSO) δ 195.62, 172.48, 149.67, 147.27, 146.94, 143.18, 140.51, 138.15, 137.66, 136.77, 134.22, 133.13, 132.70, 131.90, 129.83, 128.87, 119.55, 114.27, 113.27, 21.52(AcOH); MALDI-TOF: m/z calcd for $C_{21}H_{12}N_4O_3$ 384.08 (M^+), found 386.11.

2.8.4. (8-Chloro-6H-indolo[2,3-b]quinoxalin-3-yl)(phenyl)methanone (3d)

Yield: 74%; Colour: Yellow solid; M.P: 313°C; FT-IR (KBr): 3179 (NH Str), 2922, 2851, 1718 (C=O Str), 1629 (C=N Str), 1586, 1466, 1319, 1266, 1185, 706 cm^{-1}; ^{1}H NMR (400 MHz, DMSO-D_6): δ 10.71 (s, 1H NH), 7.71 (s, 2H CH), 7.56 (m, 1H CH), 7.43 (m, 1H CH), 7.37 (d, 2H CH), 7.25 (m, 2H CH), 6.97 (m, 1H CH), 6.90 (d, 1H CH); ^{13}C NMR (400 MHz, DMSO-D_6): δ 195.20, 155.47, 154.93, 148.00, 147.92, 143.05, 141.09, 137.91, 137.74, 137.51, 137.32, 137.23, 135.50, 134.83, 133.59, 133.39, 133.21, 132.84, 132.39, 131.73, 130.24, 130.05, 129.11, 127.05, 124.41, 118.93, 118.49, 117.17, 114.42; MALDI-TOF: m/z calcd for $C_{21}H_{12}ClN_3O$ 357.06 (M^+), found 360.14.

2.8.5. Acenaphtho[1,2-b]quinoxalin-9-yl(phenyl)methanone (3e)

Yield: 83%; Color: Primrose Yellow solid; M.P: 246°C; FT-IR (KBr): 3042, 1658 (C=O Str), 1633, 1597 (C=N Str), 122, 896, 710 cm^{-1}; ^{1}H NMR (400 MHz, DMSO-D_6): δ 8.31 (m, 6H Ar-H), 7.91 (dd, 1H CH), 7.71 (m, 4H Ar-H), 7.57 (m, 4H Ar-H); ^{13}C NMR (400 MHz, DMSO-D_6): δ 195.22, 147.99, 141.65, 137.84, 137.36 135.30, 133.30,132.83, 130.34, 129.98, 129.83, 129.49, 128.29, 127.07,124.40,118.76, 117.17, 114.44,113.01; MALDI-TOF: m/z calcd for $C_{25}H_{14}N_2O$ 358.11 (M^+), found 360.14.

2.8.6. (2,3-Diphenylquinoxalin-6-yl)(phenyl)methanone (3f)

Yield: 83%; Color: Crystalline Brown solid; M.P: 294°C; FT-IR (KBr): 3054, 1659 (C=O Str), 1596 (C=N Str), 1444, 1346, 1267, 816, 691cm^{-1}; ^{1}H NMR (400 MHz, DMSO-D_6) δ 8.36(d, 1H CH), 8.31 (d, 1H CH), 8.20 (dd, 1H CH), 7.87(d, 2H CH), 7.75 (m, 1H CH), 7.63 (m, 3H CH), 7.51 (m, 4H Ar-H), 7.39 (m, 6H Ar-H); ^{13}C NMR (400 MHz, DMSO) δ 195.28, 155.23, 154.67, 142.57, 139.89, 138.80, 138.78, 138.34, 137.08, 133.55, 131.82, 130.27, 130.22, 129.95, 129.87, 129.52, 129.17,128.57, 128.55; MALDI-TOF: m/z calcd for $C_{27}H_{18}N_2O$ 386.14 (M^+), found 388.17.

2.8.7. (5-Hydroxybenzo[a]phenazin-9-yl)(phenyl)methanone (3g)

Yield: 59%; Color: Orange solid; M.P: 289°C; FT-IR (KBr): 3042, 1658 (C=O Str), 1633, 1597 (C=N Str), 1536, 1480, 1322, 1142, 710 cm^{-1}; ^{1}H NMR (400 MHz, DMSO-D_6): δ 11.71 (s, 1 OH), 9.30 (s, 1H CH), 8.35 (dd, 3H Ar-H), 8.16 (d, 1H CH), 7.93 (m, 4H Ar-H), 7.76 (t, 1H CH), 7.65 (d, 2H CH), 7.20 (s, 1H CH). ^{13}C NMR (400 MHz, DMSO-D_6): δ 194.13, 161.60 (C-OH), 143.61, 139.37, 131.65, 129.31, 128.67, 127.32, 126.64, 125.51, 120.48, 114.05; MALDI-TOF: m/z calcd for $C_{23}H_{14}N_2O_2$ 350.10 (M^+), found 352.02.

2.8.8. 7-Benzoylbenzo[g]pteridine-2,4(1H,3H)-dione (3h)

Yield: 89%; Color: Yellow solid. M.P: 292°C; FT-IR (KBr): 3349, 1660 (C=O Str), 1646 (C=N Str), 1597, 1487, 1283, 704 cm^{-1}; ^{1}H NMR (400 MHz, DMSO-D_6): δ 11.32, 9.82 (s, 2NH), 8.26 (s 1H CH), 8.12 (s, 1H CH), 7.63 (d, 1H CH), 7.42 (d, 1H CH), 7.19 (m, 4H Ar-H); ^{13}C NMR (400 MHz, DMSO-D_6): δ 195.92, 152.56, 140.39, 138.03, 137.16, 136.84, 132.72, 130.00, 129.91, 129.36, 129.00,117.97,115.22; MALDI-TOF: m/z calcd for $C_{17}H_{16}N_4O_3$ 318.07 (M^+), found 318.08.

2.8.9. 6-Benzoylquinoxaline-2,3(1H,4H)-dione (3i)

Yield: 89%; Color: Yellow solid. M.P: 3177°C; FT-IR (KBr): 3354, 2607, 1655 (C=O Str), 1623(C=N Str), 1571, 1517, 1454, 1331, 1295, 759 cm^{-1}; ^{1}H NMR (400 MHz, DMSO-D_6): δ 7.63 (s, 1H), 7.60 (d, 2H), 7.56 (d, 1H), 7.51 (d, 3H), 7.03 (d, 2H), 6.64 (d, 2H NH); ^{13}C NMR (400 MHz, DMSO-D_6): δ 194.47, 162.48, 142.30, 139.77, 132.25, 131.40, 129.29, 128.56, 125.66, 124.28, 117.35, 113.13, 40.51, 40.30, 40.09, 39.88, 39.67, 39.46, 39.25; MALDI-TOF: m/z calcd for $C_{15}H_{10}N_2O_3$ 266.09 (M^+), found 266.07.

3. Results and discussion

3.1. Synthesis of benzyl indenoquinoxaline and optimization of reaction conditions

The synthesis of novel 8-benzoyl -11*H*-indeno[1,2-b]quinoxaline-11-one (3a) has been achieved by the cyclocondensation process of 3,4- diaminobenzophenone (1) (1.0 mmol) with ninhydrin (2a) (1.0 mmol) as model substrates under neat conditions at room temperature. The product was separated in good yields and purified by recrystallization. Similar procedures were also followed for the synthesis of other derivatives. All these compounds are yellow-orange crystalline solids, resulting as air-stable and non-hygroscopic products. They are soluble in THF, DCM, acetonitrile, acetone, toluene, 1,4-dioxane, and DMSO and sparingly soluble in chloroform and methanol.

The reaction of 2-fold excess of isatin with 3,4-diaminobenzophenone afforded compound imidazo[1,2-c]quinazoline as a sole product. An unexpected five membered heterocyclic compound was formed when an electron-withdrawing substituent is present in isatin, such as nitroisatin in the formation of imidazoquinazoline. All the synthesized compounds were analyzed by analytical techniques such as ^{1}H NMR, ^{13}C NMR, IR, and electronic spectroscopy, as well as mass spectrometry. The structure of compounds 3a and 3f was also described by single-crystal XRD methods.

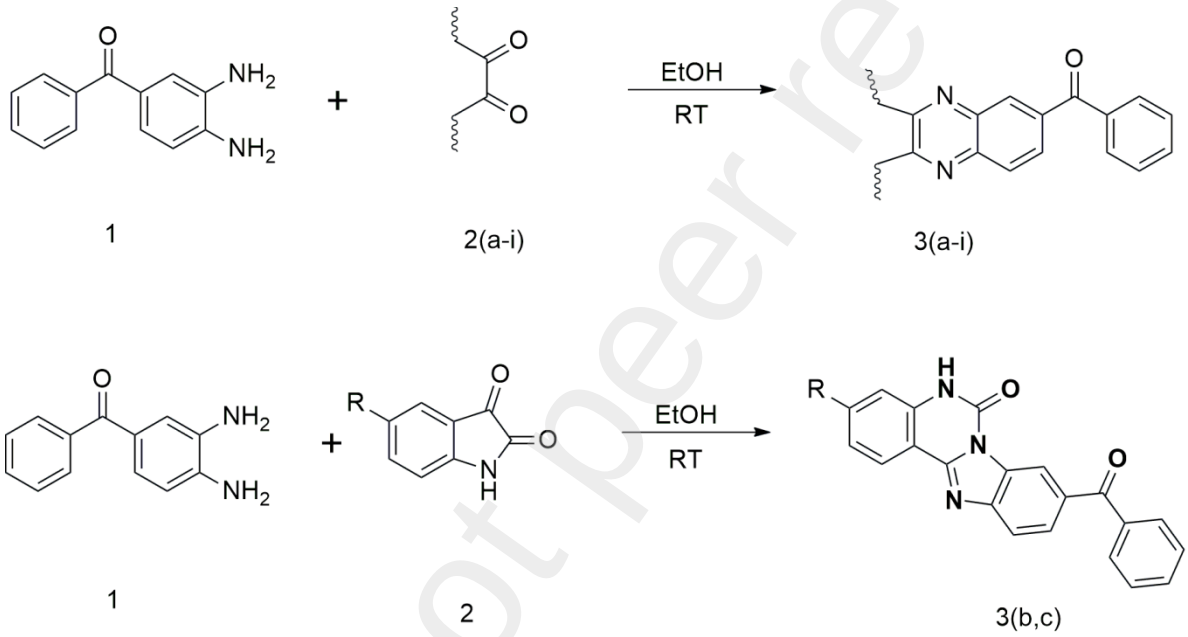

Scheme 1: Preparation of 8-benzoyl -11*H*-indeno[1,2-b]quinoxaline-11-one

The model one pot two component condensation of 3,4- diaminobenzophenone (1) (1.0 mmol) with ninhydrin (2a) (1.0 mmol) was used for various optimization studies. Initially the reaction was performed in solvents of different polarity, such as ethanol, methanol, PEG-300, ethylene glycol, diethyleneglycol, acetonitrile, DMF, and dioxane as shown in the Table-1. The resulting yield was found to be 98% in ethanol after 3h (Table-1, Entry 2), when compared to the other solvents where, the yields were moderate (20 to 78%) at room temperature.

Table-1: Optimization of an appropriate Solvent (a).

S. No	Solvent	Temp (°C)	Time (h)	Yield %[b]
1.	Water	RT	6	15
2.	**Ethanol**	**RT**	**3**	**98**
3.	Ethanol: Water	RT	4	43
4.	Methanol	RT	3	78
5.	Methanol: Water	RT	4.5	37
6.	Acetonitrile	RT	8	20
7.	PEG	RT	5	21
8.	Glycerol	RT	12	-

[a]***Reaction conditions****: 3,4- diaminobenzophenone (1.0 mmol) and ninhydrin (1.0 mmol) with different solvents (10.0 ml) at room temperature.* [b]*Isolated yields.*

The effect of temperature on the reaction time and the yields of products show that the reaction was strongly influenced by the temperature. Consequently, we have made efforts to increase the percentage of yield by optimizing the temperature suitable for the reaction by changing the conditions from room temperature to reflux conditions. It was observed that the room temperature conditions afforded better yield of 98% with reaction time of 3 h in ethanol (Table-2, Entry 1). Increase in temperature by 10 °C up to 80 °C did not show any increase in the product yield and on contrary the yield decreases with increase in the temperature.

Table-2: Optimization of appropriate Temperature (°C).

S. No	Solvent	Temp (°C)	Time (h)	Yield % [b]
1.	**Ethanol**	**RT**	**3**	**98**
2.	Ethanol	40	3	78
3.	Ethanol	50	3	72
4.	Ethanol	60	3	68
5.	Ethanol	65	3	55
6.	Ethanol	70	3	40
7.	Ethanol	80	3	38
8.	Ethanol	Reflux	3	35

[a]***Reaction conditions****: 3,4- diaminobenzophenone (1.0 mmol) and ninhydrin (1.0 mmol) with ethanol (10.0 ml) at different temperatures.* [b]*Isolated yields.*

Next, the model reaction was screened with different catalysts like piperidine, 2-aminopyridine, H_2SO_4, triethylamine and NaOH in order to reduce the reaction time. The reaction in the case of ethanol with piperidine as a catalyst did not yield any product even after 24h. It is evident that, with catalyst, the yield of the product was decreased (Table 3, Entry 2-6). From the above optimization studies, it was evident that the suitable condition for the formation of a good yield of product was the room temperature in ethanol without any catalyst. Further derivatives were prepared under these optimized conditions.

Table-3: Optimization of appropriate Catalyst.

S. No	Catalyst	Solvent	Temp (°C)	Time (h)	Yield % [b]
1.	**Without catalyst**	**Ethanol**	**RT**	**3**	**98**
2.	Pyridine	Ethanol	RT	6	-
3.	Acetic acid	Ethanol	RT	3	75
4.	H_2SO_4	Ethanol	RT	4	80
5.	Dioxane	Ethanol	RT	24	63
6.	Piperidine	Ethanol	RT	4.5	-
7.	L-Proline	Ethanol	RT	12	10
8.	Et_3N	Ethanol	RT	8	-
8.	NaOH	Ethanol	RT	24	-

[a]***Reaction conditions****: 3,4- diaminobenzophenone (1.0 mmol) and ninhydrin (1.0 mmol) with different catalysts in ethanol (10.0 ml) at room temperature.* [b]*Isolated yields*

Table-4: Synthesis of novel benzyl indenoquinoxaline derivatives (3a-i) using ethanol under catalyst-free condition.

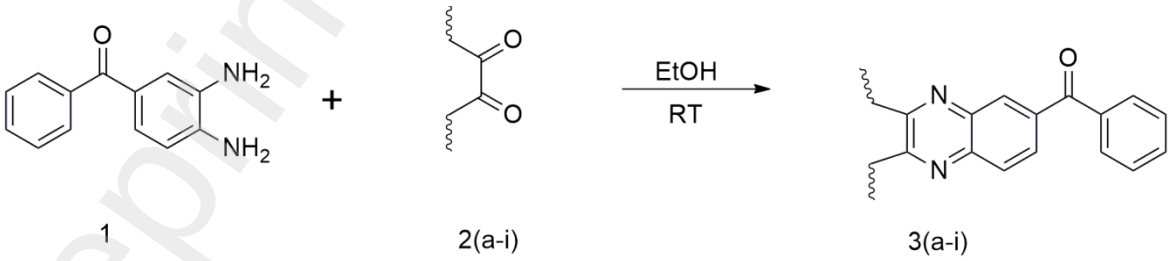

1 2(a-i) 3(a-i)

S. No	Diketone	Product	Time (h)	m.p. (°C)	Yield % [b]
1	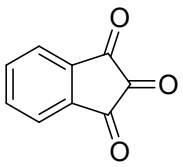	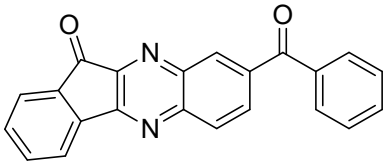	3	289	98
2	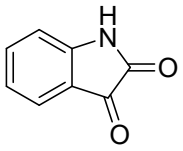	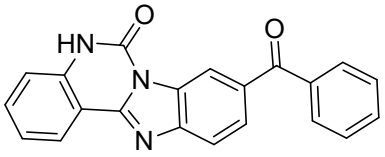	3.5	293	63
3	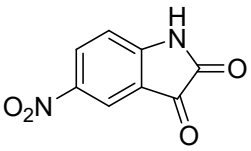	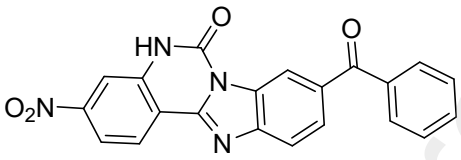	3	301	87
4	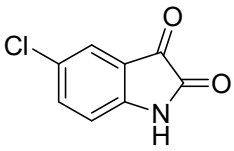	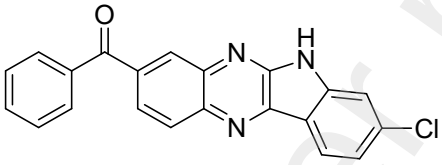	2.5	304	76
5	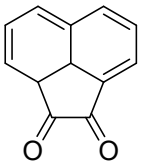	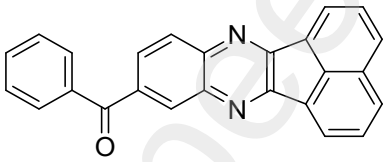	3.5	246	82
6	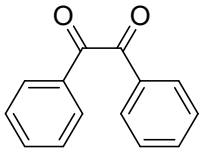	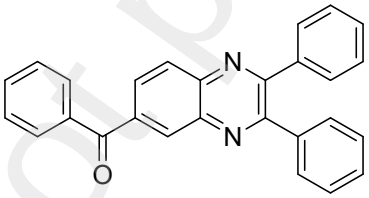	8	294	93
7	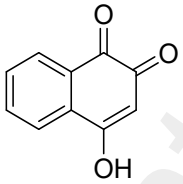	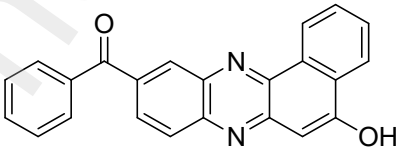	1.5	289	98
8	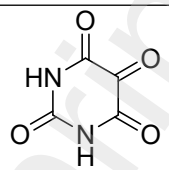	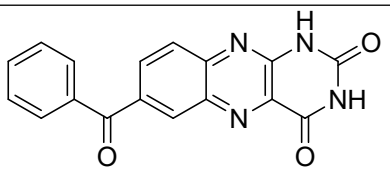	4	294	93
9	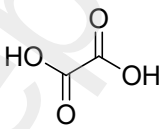	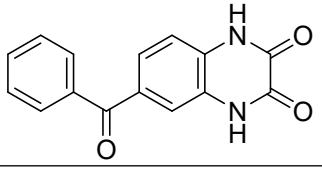	5.5	317	60

[a]***Reaction conditions***: *3,4- Diaminobenzophenone (1.0 mmol) and diketone (1.0 mmol) in ethanol (10.0 ml) at room temperature.* [b]*Isolated yields.*

3.2. Spectral studies

In the FT-IR spectrum of compounds (**3a-i**), the stretching band at 1780-1660 cm^{-1} belongs to the C=O group of BIQ. IR spectrum of all the compounds exhibit a band for the C=N Stretching frequency, around 1570-1600 cm^{-1} and compounds (**3b-d**), and (**3h-i**) showed a sharp band at 3250-3400 cm^{-1} due to the N-H stretching frequency and a band at 3339 cm^{-1} corresponding to the -O-H stretching, were also observed. The observation of a new band for C=N confirms the cyclocondensation of ninhydrin with 3,4-diaminobenzophenone.

The ^{1}H NMR spectrum of all the compounds (3a-3i) displayed aromatic protons signals at 7.7 to 8.5 ppm for the quinoxaline ring and three signals at 7.5 to 7.8 ppm for the protons of the phenyl ring. In compound (**3b**), NH proton is observed at 12.5 ppm and indolo ring protons resulted four signals at 6.5 to 8.2 ppm. NH proton signals for the compounds **(3c)** and **(3d)** are observed at low field around 10.7, 12.7 ppm respectively. In compound (**3g**), the OH proton was observed at 11.71 ppm. Compound (**3h**) showed two NH protons at around 11.3 ppm.

The ^{13}C NMR spectrum of all the compounds (**3a-i**) showed a signal at δ 194.87 ppm which is assigned to the carbonyl group of 8-benzoyl -11*H*-indeno[1,2-b]quinoxaline and a signal at δ 155.42 ppm corresponds to C=N group of quinoxaline ring. In compound (**3i**), a signal at δ 165.08 ppm was assigned to the carbon of C-OH in the hydroxynaphthoquinone ring. The aromatic carbon signals were found in the range of δ 128.0 ppm to 148.8 ppm. In the ^{13}C NMR spectrum of compounds **3(b-c)**, the carbonyl carbon atom resonated as a singlet as 149.80 and 172.48 ppm, as characteristic of a urea fragment.

The mass spectra of all the compounds (**3a-i**) exhibited their [M^{+}] molecular ion peaks matching with the theoretically expected values. The quinoxaline compounds **3(a–i)** showed their [M^{+}] molecular ion peaks at m/z 338.0754, 340.1846, 386.1140, 360.1414, 360.1414, 388.1732, 350.1756, 318.0854, 266.0794 respectively.

3.3. X – Ray Crystallographic studies

Molecular structure of benzyl indenoquinoxaline compounds (3a) and (3f) were confirmed by single crystal XRD method. The suitable crystals for X-ray crystallographic analysis were obtained by slow evaporation of benzyl indenoquinoxaline compound in ethyl acetate/THF. Crystallographic details are summarized in (Table-5). The selected bond lengths and angles are presented Table-6 & 7. Molecular structure of compounds **3a** & **3f** were drawn with ORTEP-3 and showed in Fig-1 and 2. Compound **3a** and **3f** are crystallized in the monoclinic with the space group P1 21/n1. The X-ray structure analysis of compounds **3a** and **3f** have showed that, 3,4-diaminobenzophenone condense with ninhydrin or benzil to form quinoxaline compounds as confirmed by bond lengths of C=N 1.2989 & 1.3092 (**3a**) and 1.364 & 1.366 (**3f**) and are in good agreement with those of similar compounds reported earlier .

From the ORTEP view of the compound **3a**, it is evident that the compound is nearly planar in nature (anti-periplanar conformation) due to the torsion angle between the mean plane of the quinoxaline ring (C8/C9) and benzoyl ring (C9/C10/O2) is -152.1(1)°, -141.7(1)° & -134.8(1)° for the atoms C8-C9-C10-C19, C8-C9-C10-C18 & C7-C8-C9-O2 respectively. Moreover, intramolecular hydrogen bonds of the type C…O stacking were observed in compound **3a** between the quinoxaline moiety (C6) and oxygen atom of (O2) benzoyl moiety at bond length of 3.126 A° as shown in Fig-3.

The molecular structure of compound **3f**, reveals that the phenyl rings are located at the 2,3-position of the quinoxaline nucleus with the dihedral angles 39.12° and 50.55° while benzoyl ring is located at the 7-position of the quinoxaline moiety with the dihedral angle -47.69°. Additionally, due to steric hindrance, the average twist angle of the phenyl ring at the 2,3-position is significantly greater than the twist angle of the substituent at the 7-position. On the other hand, □–□ interactions were observed between adjacent molecules in the crystal packing with the bond distance 3.373 Å and also were connected *via* C…O (C6...O1)

interaction with bond distance of 3.064 Å. Compound 3f is a mutual chimeric stacking mode because of the high molecular interaction, as seen in Fig. 4.

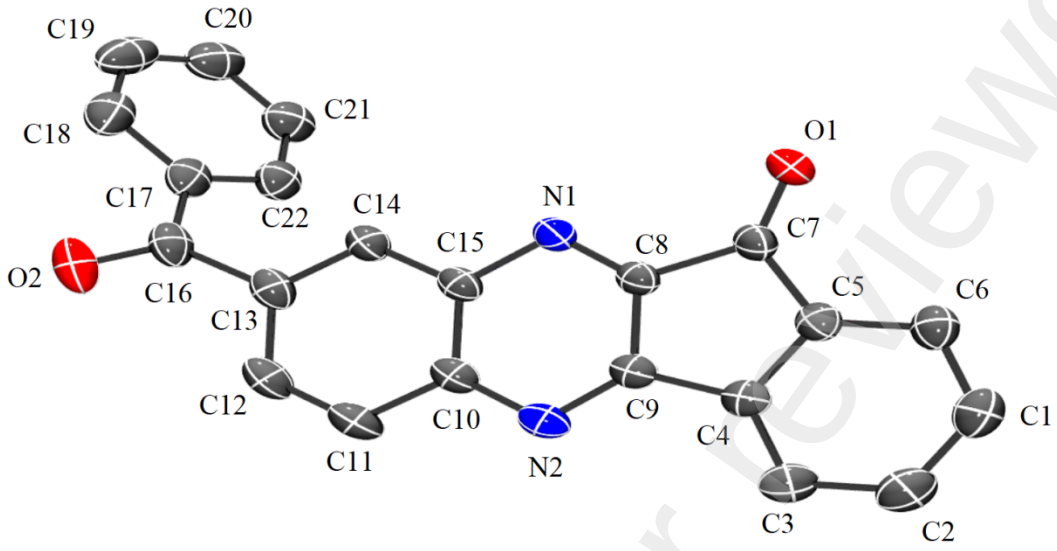

Fig-1: ORTEP diagram of compound 3a

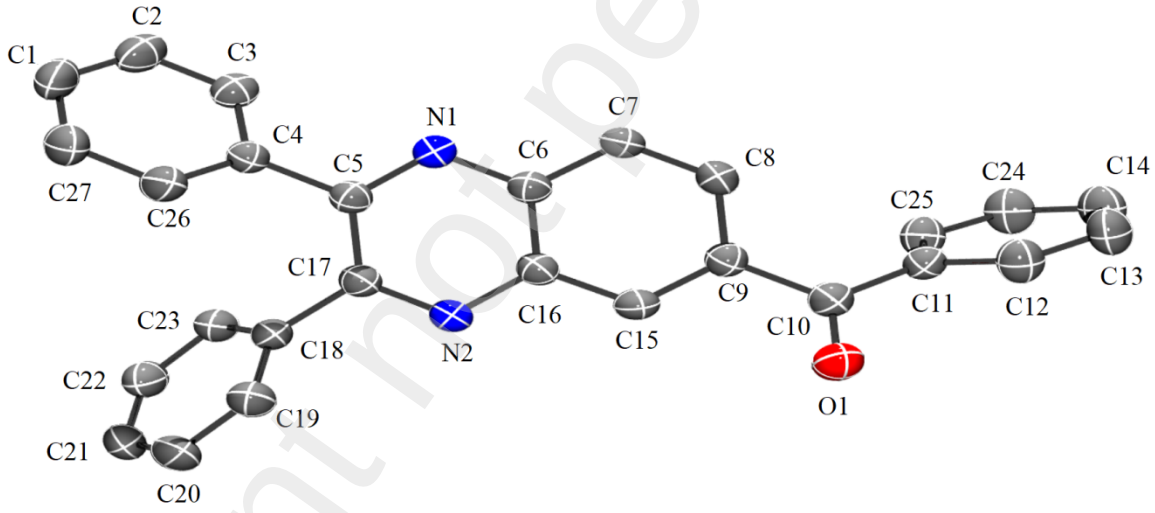

Fig-2: ORTEP diagram of compound 3f

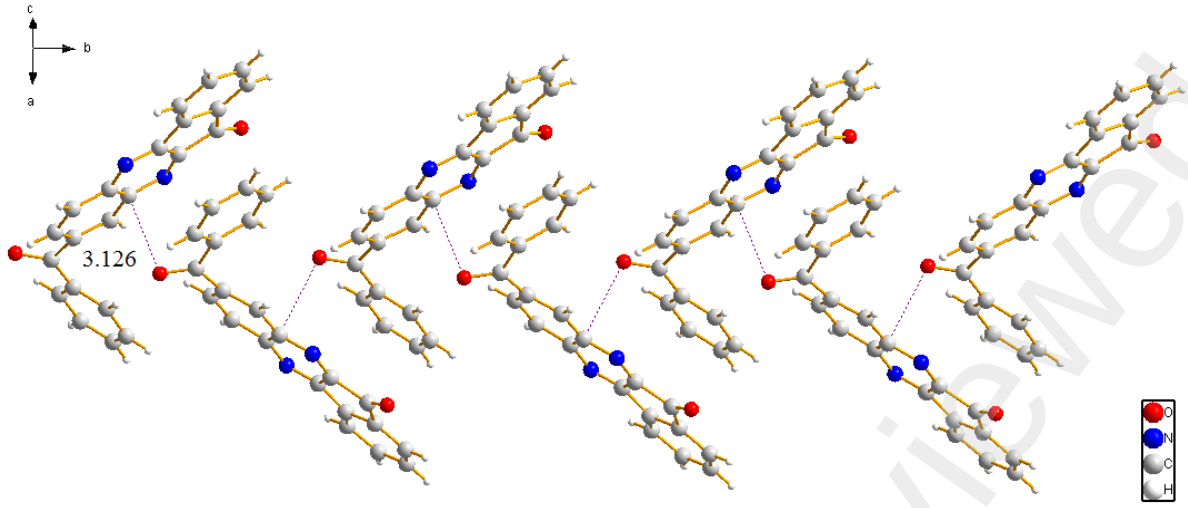

Fig-3: C…O stacking interaction of compound 3a

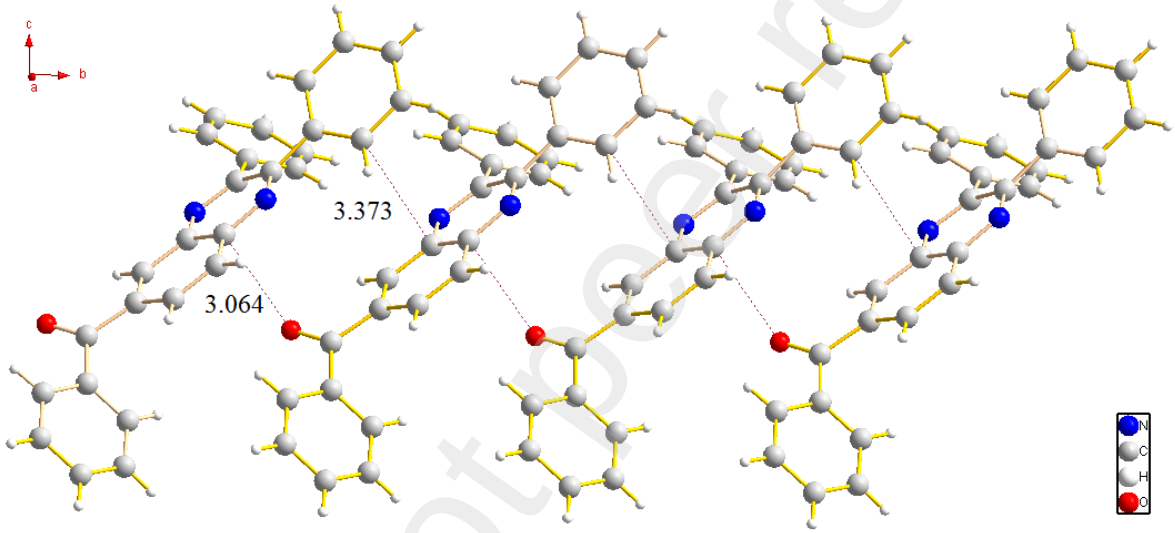

Fig-4: π….π, C…O stacking interaction of compound 3f

Table-5: Crystallographic and structure refinement parameters for compounds 3a & 3f

Compound	3a	3f
Chemical formula	$C_{22}H_{12}N_2O_2$	$C_{27}H_{18}N_2O$
Formula mass	336.08	386.43 g/mol
Crystal system	monoclinic	monoclinic
Crystal habit	fluorescent orange	fluorescent light brown block
a/Å	11.8343(3) Å	14.8221(9) Å
b/Å	10.1667(2) Å	6.1537(3) Å
c/Å	14.1209(4) Å	22.9513(15) Å
α/°	90°	90°
β/°	107.443(2)°	107.223(3)°
γ/°	90°	90°
Unit cell volume/Å3	1620.84(7) Å3	1999.5(2) Å3
Temperature/K	293 K	293 K
Space group	P 21/n	P 21/n

Z	4	4
Index ranges	-15<=h<=15, -13<=k<=13, -18<=l<=18	-18<=h<=19, -7<=k<=8, -28<=l<=28
Reflection collected	4041	3650
Independent reflections	3291[R(int) = 0.0433]	2408 [R(int) = 0.0710]
Data/ restraints/ parameters	4036 / 0 / 283	4668 / 0 / 343
Goodness-of-fit on F^2	1.053	1.000
Final R indices	3291 data; I>2σ(I) R1 = 0.0656, wR2 = 0.2146 all data R1 = 0.0433, wR2 = 0.1324	2588 data; I>2σ(I) R1 = 0.0632, wR2 = 0.1531 all data R1 = 0.1288, wR2 = 0.1443
Largest diff. peak and hole	0.300 and -0.540 eÅ-3	0.184 and -0.225 eÅ-3

Table-6: The selected bond length and bond angle of compound 3a

Atoms	Bond length		Atoms	Bond angle	
	XRD	DFT		XRD	DFT
N1-C8	1.2989 (15)	1.310	C8-N1-C15	114.1 (10)	114.4
N1-C15	1.3784 (14)	1.374	N1-C15-C14	118.4 (10)	118.7
N2-C9	1.3092 (15)	1.317	N1-C15-C10	121.7 (11)	121.8
N2-C10	1.3787 (16)	1.374	C9-N2-C10	114.2 (10)	114.4
O1-C7	1.2052 (12)	1.218	N2-C9-C8	123. 1(11)	123.5
C15-C14	1.4057 (17)	1.414	N2-C10-C11	119.3 (11)	119.3
C18-C19	1.3810 (3)	1.392	N2-C10-C15	122.2 (10)	121.1
C13-C12	1.4120 (2)	1.423	O1-C7-C5	128.2 (12)	127.8
C4-C3	1.3807(19)	1.394	N1-C8-C9	124.5 (10)	123.9
C21-H11	1.0200 (2)	1.09	O1-C7-C8	127.6(12)	127.8
C16-O2	1.2223(18)	1.231	N1-C8-C7	127.3(10)	127.6
C12-H6	0.9690(17)	1.09	O2-C16-C17	121.7(14)	120.6
C22-H12	1.021(18)	1.09	O2-C16-C13	118.7(14)	119.1

Table-7: The selected bond length and bond angle of compound 3f

Atoms	Bond length		Atoms	Bond angle	
	Exp.	DFT		Exp.	DFT
N1-C5	1.364 (3)	1.359	C5-N1-C6	117.4 (2)	118.65
N1-C6	1.327 (3)	1.327	C12-N2-C6	117.2 (2)	118.71
N2-C17	1.366 (3)	1.361	N1-C4-C6	120.9 (2)	120.39
N2-C16	1.315 (3)	1.326	N2-C6-C3	118.9 (2)	120.08
O1-C10	1.221 (3)	1.230	N2-C6-C4	121. 2 (2)	120.28
C9-C10	1.493 (3)	1.504	N2-C12-C5	121.8 (2)	120.48
C10-C11	1.490 (3)	1.500	N2-C12-C17	114.9 (2)	115.63
C4-C6	1.407(4)	1.432	O11-C13-C7	119.6 (2)	119.93
C5-C12	1.439 (4)	1.456	N1-C4-C8	120.3 (2)	120.22

3.4. DFT Studies

3.4.1. Geometric optimization

The geometry of the title compounds is optimized by the density functional theory (DFT) method at the BP86/Def2-TZVP level using the program ORCA. The optimized structure of compounds **3a** and **3f** has been shown in Fig-5 & 6. Theoretical and X-ray data for bond angles and bond distance were in Table-7 & 8, respectively. Geometry optimization of the compounds **3a** and **3f** leads to the minimum energy structure with no imaginary frequencies and confirms that optimized geometries are minimum energy structures in the potential energy surface. The DFT (BP86/Def2-TZVP) computed bond parameters of the compounds **3a** and **3f** exist in good agreement with those of the experimentally obtained X-ray diffraction data values.

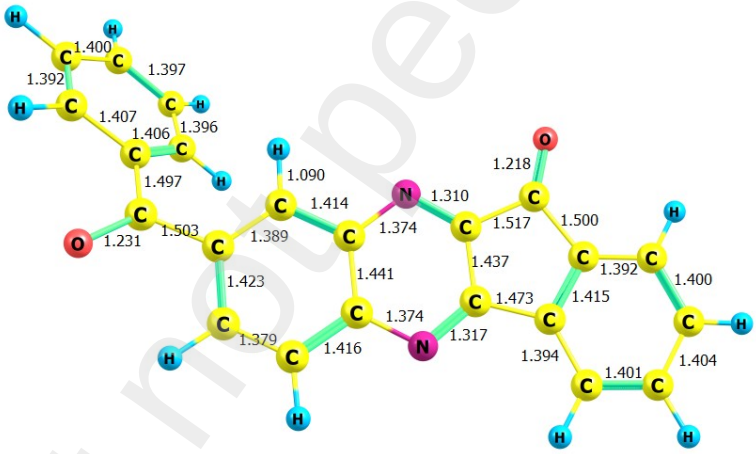

Fig-5: DFT (BP86/Def2-TZVP) Optimised geometries of compounds (3a)

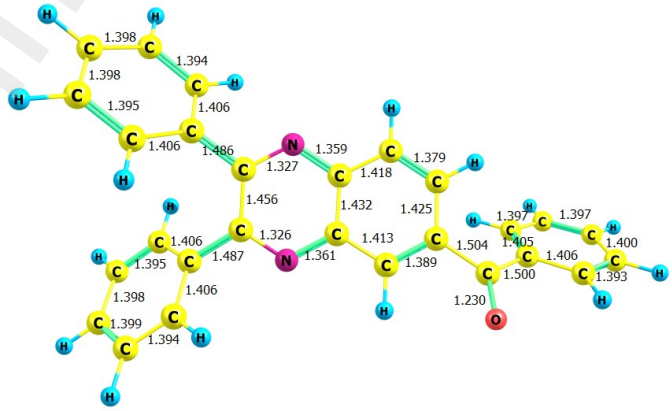

Fig-6: DFT (BP86/Def2-TZVP) Optimised geometries of compounds (3f)

3.4.2. Electronic properties/ Frontier molecular orbital analysis

Using the ORCA software, the electric properties of compounds 3a and 3f are computed at the BP86/Def2-TZVP level of theory. The HOMO and LUMO energy values are used to calculate and evaluate conceptual density functional theory properties such as global softness, electrophilicity index, chemical potential, and global hardness. The reactivity of a molecule is controlled at the molecular level by the frontier molecular orbitals (FMO), *viz.* HOMO and LUMO. The energy difference between HOMO and LUMO gives the energy of band gap which is used to predict the kinetic stability, chemical reactivity of the molecules and to determine electrical and optical properties, which are the most important parameters of quantum chemistry. The highest occupied molecular orbital and lowest unoccupied molecular orbitals of the compounds **3a** and **3f** in the gas phase are shown in Fig-7. The electronic properties of the compound **3a** and **3f** were obtained from the calculated HOMO and LUMO energies and listed in Table-8.

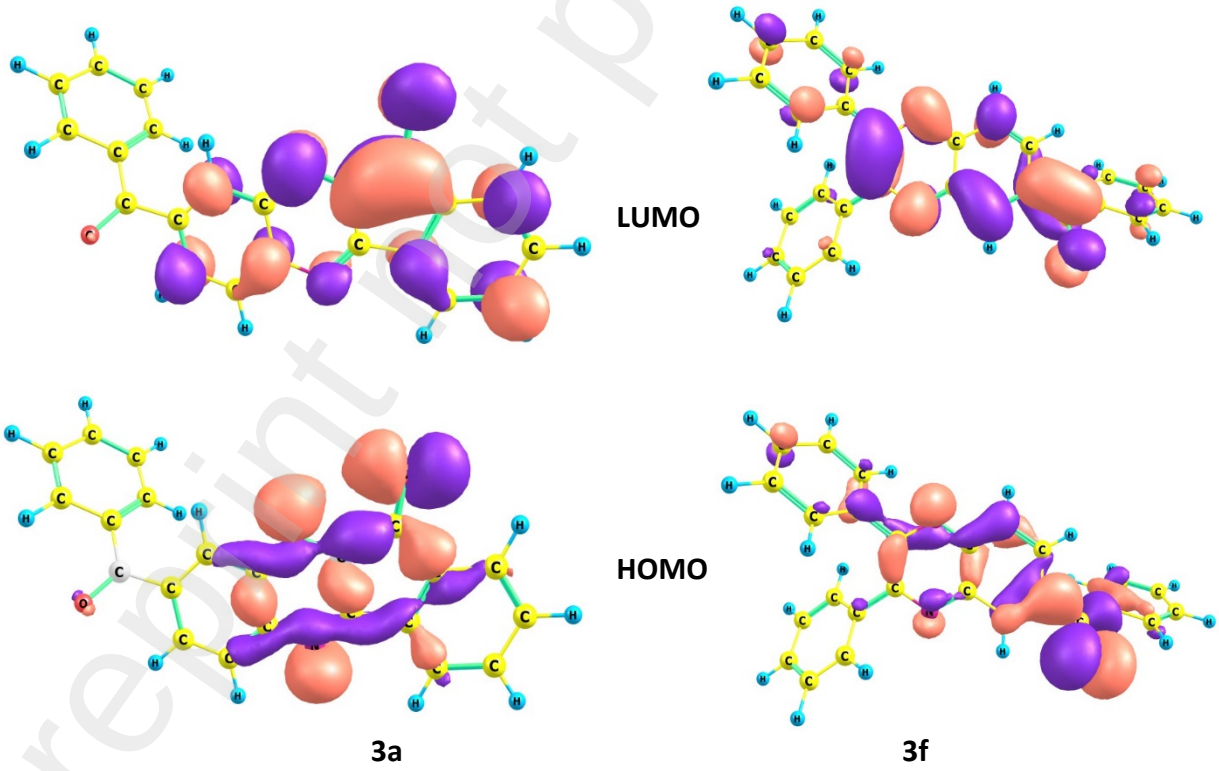

Fig-7: Frontier molecular orbitals of the compounds (3a and 3f)

Table-8: DFT (BP86/Def2-TZVP) computed electronic properties of Compounds (3a) and (3f)

Electronic Properties		Values (eV) 3a	3f
Ionization Potential	$I = -E_{HOMO}$	5.8574	5.8240
Electron Affinity	$A = -E_{LUMO}$	3.8857	3.3534
Energy Gap	$(\Delta E = (E_{LUMO} - E_{HOMO})$	1.9717	2.4706
Electronegativity	$\chi = (I + A) / 2$	4.8716	4.5887
Molecular Hardness	$\eta = (I - A) / 2$	0.9859	1.2353
Molecular Softness	$S = 1/\eta$	1.0143	0.8095
Chemical Potential	$\mu = -\chi$	-4.8716	-4.5887
Electrophilic Index	$\omega = \mu^2/2\eta$	12.0360	8.5227
Dipole Moment (Debye)		2.9465	3.0636

The compound **3a** and **3f** showed $E_{LUMO-HOMO}$ energy gap value of 1.97 eV and 2.47eV, respectively confirming the more stable nature of **3f** when compared to **3a**. The molecule's ability to donate electrons is shown by the EHOMO value in HOMO-LUMO energy, whereas its ability to accept electrons is indicated by the ELUMO value. Compared to molecules having a high energy gap, those with a smaller energy gap have more chemical reactivity. The electrophilicity index values of **3a** and **3f** confirm the more electrophilic nature of the compound **3a** (12.04 eV) when compared to that of **3f** (8.02 eV).

3.4.3 ^{1}H and ^{13}C NMR spectral studies

Computational chemistry tools like DFT methods can also be used to predict the isotropic magnetic shieldings of the atoms individually and can assist the ^{1}H and ^{13}C spectral assignments. This method can aid if there is a mixture of isomers or trivial hydrogen atoms, bridging hydrogen atoms etc., Gauze Induced Atomic Orbital (GIAO) method has been used to compute the isotropic magnetic shielding of the compounds **3a** and **3f**. The isotropic magnetic shielding are then used to calculate the chemical shift values of the individual atoms by considering the tetramethylsilane as reference. The DFT (Def2-TZVP) compute ^{1}H and ^{13}C NMR chemical shift values for compound **3a** is given in the Table-9.

Experimentally nineteen ^{13}C NMR signals were obtained for the twenty two carbon atoms of the compound **3a**. The DFT method was useful to assign the chemical shift values of the twenty two carbon atoms individually and the DFT computed values are in close agreement with those of the experimentally by obtained ^{13}C and ^{1}H chemical shift values (Table-9 and Fig-8). In the ^{13}C NMR spectra the two carbonyl carbon atoms resonate at 194.87 ppm and 197.7 ppm respectively. In the ^{1}H NMR spectra eight signals are obtained for the twelve hydrogen atoms. DFT methods predict the chemical shift values for the individual hydrogen atoms. From DFT computations, among the five hydrogen atoms of the phenyl ring attached to carbonyl group, four resonate around 7.6 to 7.8 ppm and the remaining hydrogen atom which is spatially close to C=O group resonate at 8.46 ppm.

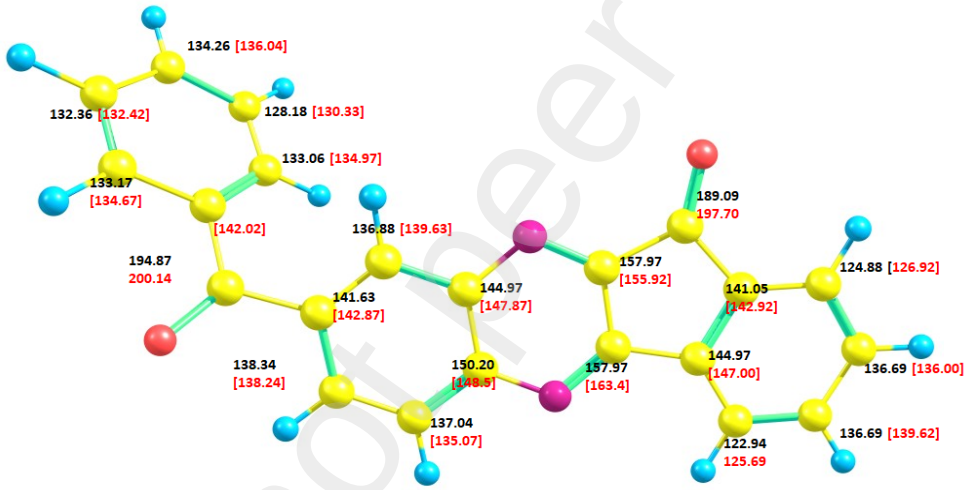

Fig- 8: The DFT (Def2-TZVP) computed ^{13}C NMR chemical shift values for compound 3a are provided in the square brackets along with experimental values.

Table-9: The DFT (Def2-TZVP) computed ^{1}H and ^{13}C NMR chemical shift values for compound 3a. Experimental values are given and DFT computed values are in square brackets.

Atoms	Chemical Shift ppm	Atoms	Chemical Shift ppm
^{13}C NMR		C34	132.36 [132.42]
C5	136.69 [136.0]	C36	144.97 [147.0]
C7	124.88 [126.92]	C37	122.94 [125.69]
C9	141.05 [142.92]	C32	133.17 [134.67]
C10	189.09 [197.7]	C30	138.34 [138.24]

C11	157.97 [155.92]	^{1}H NMR	
C12	144.97 [147.87]	H6	[7.677]
C13	136.88 [139.63]	H8	[7.93]
C15	141.63 [142.87]	H14	[8.573]
C16	194.87 [200.14]	H19	[7.988]
C17	[142.02]	H21	[7.658]
C18	133.06 [134.97]	H23	[7.802]
C20	128.18 [130.33]	H25	[7.808]
C22	134.26 [136.04]	H29	[8.352]
C24	139.69 [139.62]	H31	[8.696]
C26	157.97 [163.4]	H33	[8.462]
C27	150.20 [148.5]	H35	[7.811]
C28	137.04 [135.07]	H38	[8.271]

3.5. Molecular Docking

Molecular docking studies demonstrate both ligand-protein interaction and the effectiveness of probe molecules in preventing diseases. To assess the synthetic drugs' binding affinities and inhibitory mechanisms, molecular docking studies were conducted using the chosen protein as the host. Induced-fit docking is the best method for determining the binding affinity between a ligand and an enzyme because of the flexibility of both throughout the docking process. A number of intermolecular interactions involving amino acid residues were used to determine the synthesized compounds 3(a-i) binding affinity. 3D Structure of compound 3i and its interaction with amino acid 4HJO is provided in Fig. 9(a) whereas the 2D Structures of compound 3i the ligand interaction with amino acid 4HJO is given in Fig.9 (b). The quinoxaline ring occupied the hydrophobic pocket II enclosed by frequently LEU residues as van der Waals bonding interaction with: GLUA:443, PHEA:452, GLUA:179, HISA:133, PHEA:321, THRA:319, ASPA:246 and covalent hydrogen bonding interaction with GLNA:32, TRPA:444, and a docking score of -9.08 kcal/mol. In summary, the theoretical *in-silico* molecular docking scores provided strong evidence for the bacterial inhibitors. The results of the *in vitro* antibacterial activity studies were found to be in good arrangement with the theoretical values obtained with the molecular docking.

Table-10: Intermolecular interacting residues between synthesized benzyl indeno quinoxaline derivatives (3a-i) with 4HJO

S. No	Compound Name	Docking Score	Hydrophobic Interactions	Hydrogen Bonds
1	3a	-6.86	GLUA:179, TRPA:436, CYSA:182, ASPA:246, HISA:270, TRPA:361, HISA:193.	TYRA:134.
2	3b	-8.72	TRPA:436, GLUA:389, CYSA:182, PHEA:452.	GLUA:179, TYRA:134.
3	3c	-8.42	PHEA:321, PHEA:344, TRPA:436, GLUA:389, TRPA:361, HISA:193, LEUA:186.	TYRA:134, TYRA:360.
4	3d	-5.83	TYRA:360, TRPA:361, TRPA:436, TYRA:318,LEUA:186.	ASNA:190.
5	3e	-7.73	TRPA:361, GLUA:389, CYSA:182, TYRA:436,CYSA:182,VALA:248.	TYRA:360, TYRA:134.
6	3f	-8.87	PHEA:452, PHEA:344, TRPA:436, GLUA:389, GLUA:443, TYRA:318 TRPA:340, HISA:270,VALA:248.	TYRA:134.
7	3g	-6.53	VALA:248, HISA:270,ARGA:181.	TYRA:250, TYRA:134.
8	3h	-6.99	GLUA:179, TRPA:361, GLUA:389, HISA:193, CYSA:182, TYRA:436.	TYRA:360, TYRA:134.
9	**3i**	**-9.08**	**GLUA:443, PHEA:452, TYRA:318, TRPA:436,GLUA:179, TYRA:134, TRPA:361, HISA:133, PHEA:321, THRA:319, ASPA:246.**	**GLNA:32, TRPA:444.**

(a) (b)

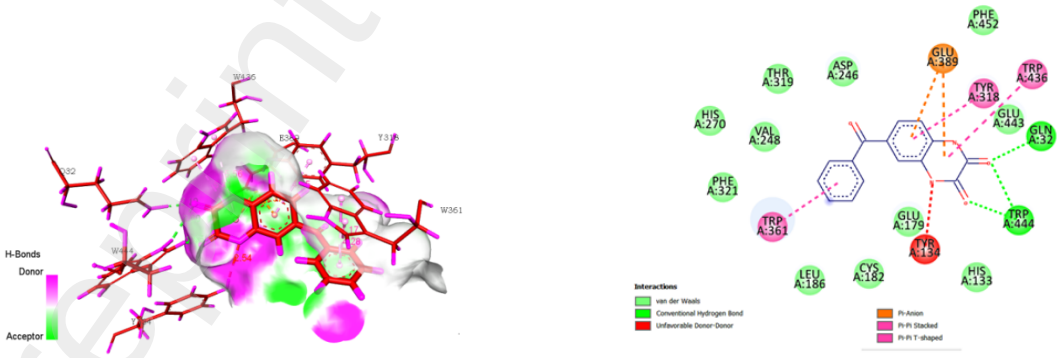

(c)

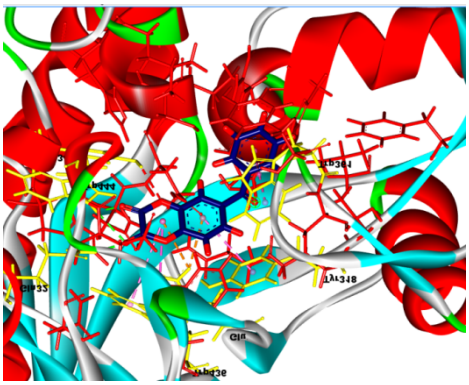

Fig-9: a) 3D Structure b) 2D Structure c) Ribbon view of compound 3i and its interaction with amino acid 4HJO.

3.6. ADME (absorption, distribution, metabolism and excretion) prediction

The ADME calculations were performed for the synthesized compounds (**3a–i**) for the assessment of drug pharmacokinetic and drug-like qualities. The Lipinski's rule of five predicts the oral bioavailability of a synthesized compound based on its physicochemical properties. According to this rule, a molecule will act as orally active drug if its molecular weight is less than 500 (m/z) and it should not contain more than five hydrogen bond donors and not more than 10 hydrogen bond acceptors. In addition, the lipophilicity (cLogP) should be lesser than 5. If the synthesized molecules exhibit more than one violation of the aforementioned criteria, then the compounds will not be considered as drugs.

Further, the bioavailability score, as well as certain pharmacokinetic properties for the full active and the BOILED-Egg plot of benzyl indeno quinoxaline (3a-i) using SwissADME web tool has been provided in Fig.11. The molecular weights of the synthesized compounds lie in the range 320.24-416.15, which is well within the limits prescribed by the Lipinski's rule of five. The calculations were executed using Swiss ADME software and the results stand showed in Table -11 to 13. Since all of the generated compounds exhibited good drug-likeness properties and no deviations from the Lipinski's rule of five, they may be considered appropriate for drug processing. It is fascinating to know that the parameters like the number of rotatable bonds and topological polar surface area (TPSA) are important factors of oral

bioavailability of pharmaceuticals and highly helpful physicochemical factors for predicting drug transport characteristics. Moreover, for a drug TPSA should be less than 140 Å2 and its number of rotatable bonds too less than ten as predicted by Veber rule. The formula % Abs = 109 - 0.345 × TPSA [62] was used to determine the synthesized compounds percentage of absorption.

Table-11: *In-silico* prediction of physicochemical, drug-likeness properties, and medicinal chemistry parameters for most active quinoxaline derivatives.

S. No	Compound	RB[a]	MR[b]	PHYSICOCHEMICAL PARAMETERS					LIPINSKI'S VIOLATION	% Abs
				TPSA[c] Å2	MW[d] (<500)	HBA[e] (<10)	HBD[f] (<5)	ilogPo/w[g] (<5)		
1	3a	2	98.28	59.92	336.34	4	0	3.55	0	88.3276
2	3b	2	98.78	58.64	323.35	3	1	3.90	0	88.7692
3	3c	2	103.79	58.64	357.79	3	1	4.44	0	88.7692
4	3d	2	106.45	63.08	350.37	4	1	4.11	0	87.2374
5	3e	2	111.35	48.85	358.39	3	0	4.77	0	92.1468
6	3f	4	120.28	42.85	386.44	3	0	5.23	0	94.2168
7	3g	2	88.16	108.57	318.29	5	2	1.90	0	71.5434
8	3h	2	75.29	75.93	264.24	5	0	1.38	0	82.8042
9	3i	4	129.89	85.70	440.45	6	0	4.55	0	79.4335

[a] Number of rotatable bonds; [b] molar refractivity; [c] topological polar surface area; [d] molecular weight; [e] hydrogen bond acceptors; [f] hydrogen bond donors; [g] ilog$P_{o/w}$, in-house physics-based method implemented for the calculation of lipophilicity.

Table 12: *In-silico* prediction of lipophilicity parameters for most active quinoxaline derivatives.

S. No	Compound	LIPOPHILICITY PROPERTIES				
		LogPo/w (iLOGP)	LogPo/w (XLOGP3)	LogPo/w (WLOGP)	LogPo/w (MLOGP)	LogPo/w (SILOCOS-IT)
1	3a	2.46	4.06	4.07	2.16	4.98

2	3b	2.60	4.44	4.50	3.12	4.87
3	3c	2.87	5.06	5.15	3.60	5.50
4	3d	2.83	4.87	4.87	3.11	4.87
5	3e	3.36	5.20	5.66	3.54	6.07
6	3f	3.73	5.87	6.19	3.91	6.43
7	3g	1.35	1.74	1.39	1.52	3.50
8	3h	1.17	1.31	-0.54	0.96	4.01
9	3i	3.34	5.27	5.19	3.30	5.67

Table-13: *In-silico* pharmacokinetic properties and toxicity prediction of the quinoxaline derivatives as well as standard drugs.

S. No	Compound	PHARMACO-KINETICS PROPERTIES							
		GI absorption	BBB permeant	P-gp substrate	CYP1A2 inhibitor	CYP2C19 inhibitor	CYP2C9 inhibitor	CYP2D6 inhibitor	CYP3A4 inhibitor
1	3a	High	Yes	No	Yes	Yes	Yes	No	Yes
2	3b	High	Yes	Yes	Yes	Yes	No	Yes	Yes
3	3c	High	Yes	Yes	Yes	Yes	Yes	No	Yes
4	3d	High	Yes	Yes	Yes	Yes	No	No	No
5	3e	High	Yes	Yes	Yes	Yes	No	No	No
6	3f	High	No	Yes	Yes	Yes	No	No	Yes
7	3g	High	No	No	No	No	No	No	No
8	3h	High	No	No	Yes	Yes	No	No	No
9	3i	High	No	No	No	Yes	Yes	No	No

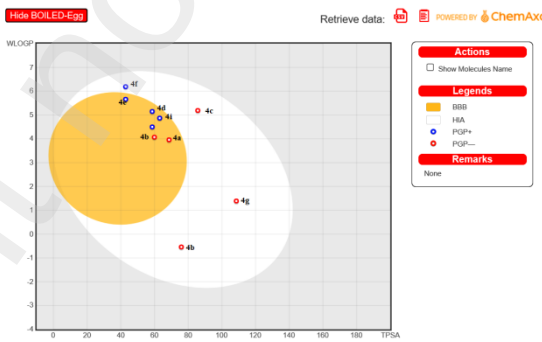

Fig-10: BOILED-Egg plot of benzyl indenoquinoxaline (3a-i) using SwissADME web tool.

3.7. Anti-bacterial activity

The newly synthesized benzyl indenoquinoxaline derivatives 3(a-i) exhibited a varying pattern of inhibition against the tested microorganisms which are shown in Table-14.

Klebsiella pneumoniae showed the highest zone of inhibition, while *Staphylococcus aureus* and *Escherichia coli* exhibited the lowest zone of inhibition. Compounds **3h** and **3i** from the series showed excellent antibacterial activity against *Klebsiella pneumoniae*, while the remaining compounds showed moderate antibacterial activity against all tested bacterial strains, including *Klebsiella pneumoniae, Escherichia coli,* and *Staphylococcus aureus*. From the above results it can be inferred that by altering the appropriate R in the benzyl indenoquinoxaline derivatives it may lead to a promising antibacterial agent.

Table-14: Antibacterial activity of novel benzyl indeno quinoxaline derivatives 3(a-i)

S. No	compounds	*E. Coli* (mm)			*S. aureus* (mm)			*Klebsiella* (mm)		
		10 µl	20 µl	30 µl	10 µl	20 µl	30 µl	10 µl	20 µl	30 µl
1	3a	4	5	4	3	3	3	5	5	5
2	3b	2	2	2	1	1	1	3	3	3
3	3c	Nil	Nil	Nil	Nil	Nil	Nil	1	1	1
4	3d	Nil	Nil	Nil	1	1	4	Nil	Nil	Nil
5	3e	Nil	Nil	Nil	Nil	Nil	Nil	Nil	Nil	Nil
6	3f	Nil	Nil	Nil	5	5	6	Nil	Nil	Nil
7	3g	Nil	Nil	Nil	Nil	Nil	Nil	Nil	Nil	Nil
8	3h	Nil	Nil	Nil	Nil	Nil	Nil	15	15	15
9	3i	2	2	2	Nil	Nil	Nil	4	3	3
10	*Streptomycin* Standard (drug) *(25 µg/mL of DMSO)*	15			15			15		

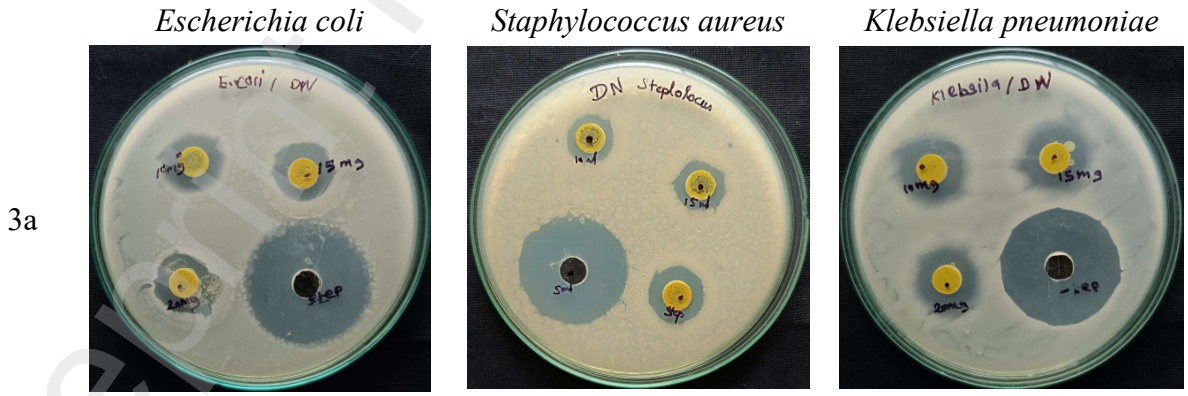

3b

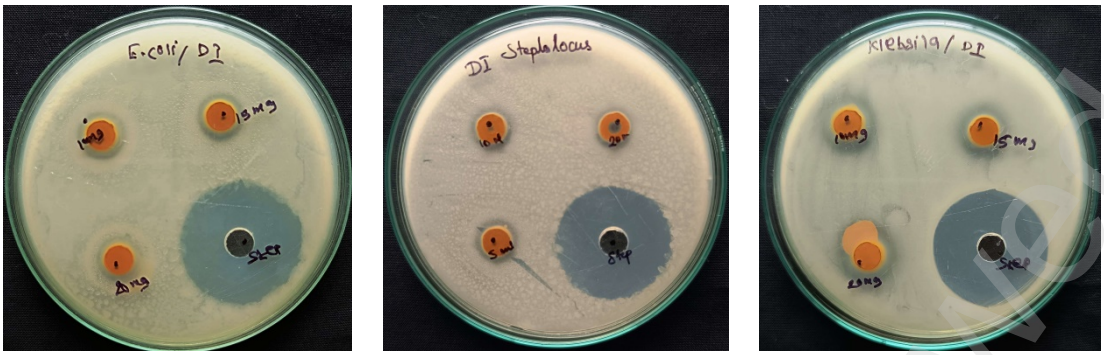

3c

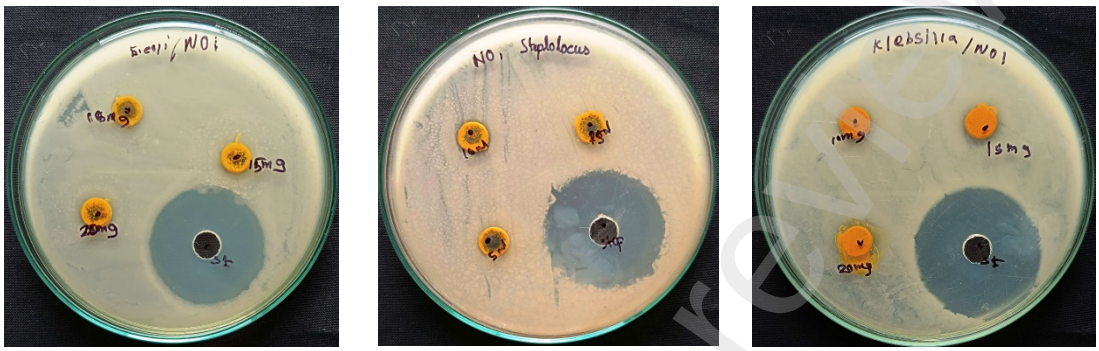

3d

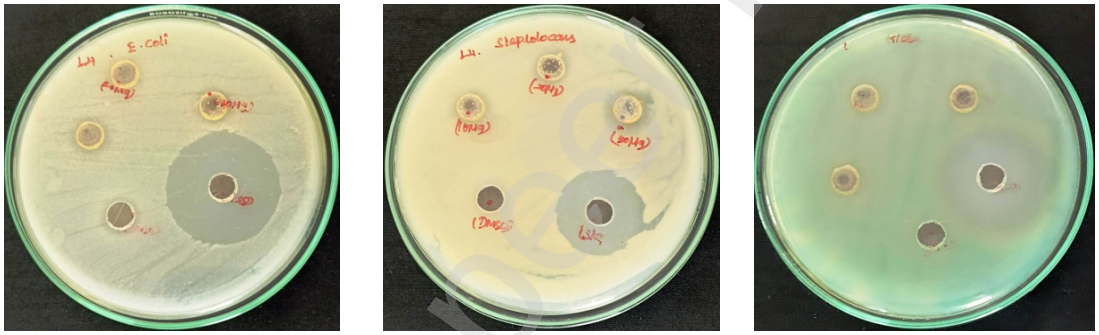

3e

3f

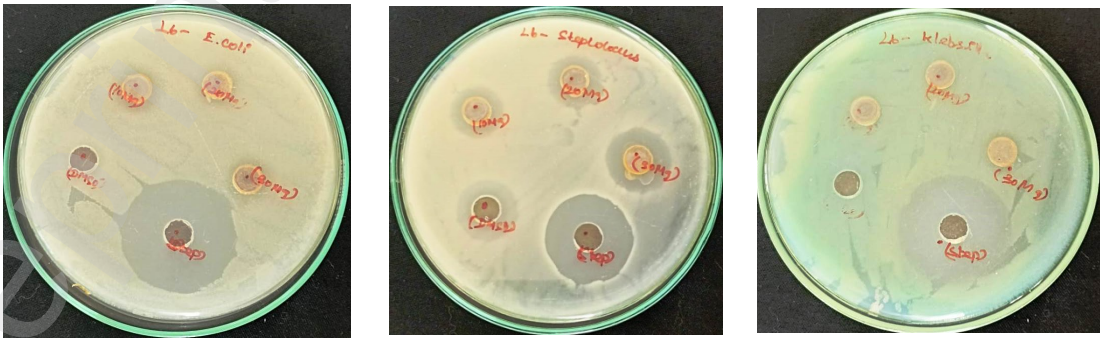

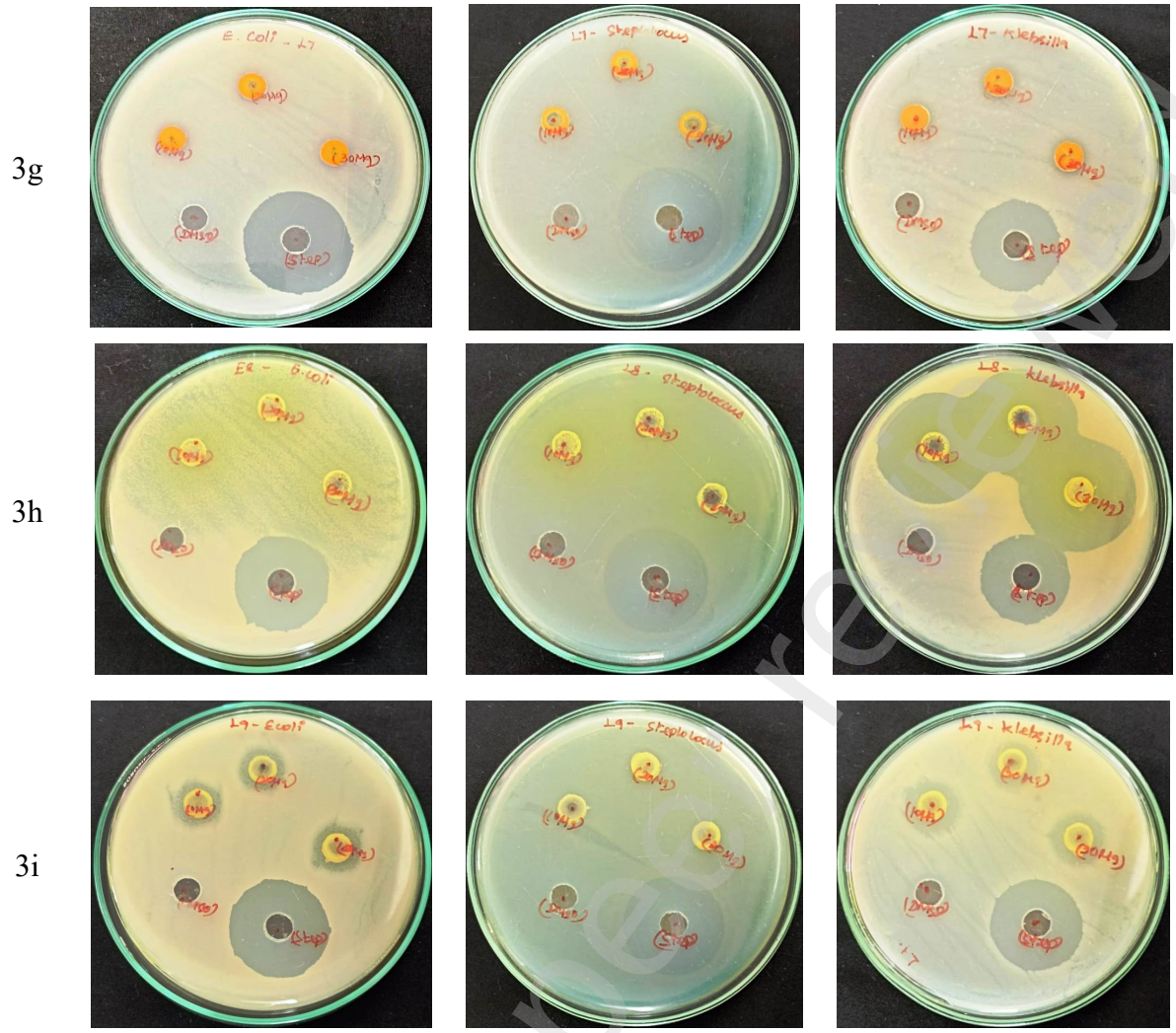

Fig -11: Antibacterial activity of all the quinoxaline derivatives 3(a-i) against *Escherichia coli, Staphylococcus aureus, Klebsiella pneumoniae.*

4. Conclusion

An efficient and convenient synthesis of 8-benzoyl-11*H*-indeno[1,2-b]quinoxaline 11-one under catalyst free condition has been achieved. The present method has notable advantages such as, one step method using broad scope, simple separation of the product and green solvent conditions without any chromatographic techniques. In this present study, functionalized derivatives of benzyl indenoquinoxaline were successfully synthesized. The structure of the compounds **3a** and **3f** were confirmed by the X-ray diffraction method, and the band distance, bond angles, and IR spectral data were compared with theoretical values by DFT methods. Moreover, these compounds have been examined by molecular docking studies and ADME studies that showed more effective binding with protein 4HJO. From antibacterial studies, the compound **3h** was found to have high antibacterial activity.

Declaration of competing Interest

The authors declare that they have no known competing financial interests or personal relationship that could have appeared to influence the work reported in this paper.

Acknowledgments

The authors gratefully acknowledges Periyar University, Salem for the Single crystal X- Ray facility and also acknowledges NMR Facility, The Gandhigram Rural Institute (Deemed to be university) Gandhigram, Dindigul, Tamil Nadu. We also acknowledge NMR facility, CIC, Bharathiar University supported by DST (PURSE Phase II programme), New Delhi.

CRediT authorship contribution statement

V. Rahimiya: Conceptualization, Methodology, Software, Validation, Investigation, Resources, Writing –original draft. Mahesh Kalidasan: Software, Validation, Formal analysis, Visualization. Krishnamoorthy Bellie Sundaram – Investigation, Writing & Editing. Appaswami Lalitha: Conceptualization, Validation, Investigation, Writing- review & editing, Supervision, Project administration

Supplementary materials

CCDC: 2366306 (DOI: 10.5517/ccdc.csd.cc2kfbgt) and 2366112 (DOI: 10.5517/ccdc.csd.cc2kf46c) comprise the supplementary crystallographic data for this paper.

References

1. J. Yamaguchi, A.D. Yamaguchi, K. Itami, Angew. Chem. Int. Ed. 51 (2012), 8960-9009. doi.org/10.1002/anie.201201666
2. K. Muller, C. Faeh, F. Diederich, Fluorine in pharmaceuticals: looking beyond intuition, Science, 317 (2007), 1881-1886. doi: 10.1126/science.1131943
3. C. Vaxelaire, P. Winter, M. Christmann, Angew. Chem. Int. Ed. 50 (2011), 3605-3607. doi: 10.1002/anie.201100059
4. H. Roder, N. Krause, Angew. Chem. Int. Ed. 43 (2004), 1196-1216. https://doi.org/10.1002/anie.200300628
5. T. Tanaka, A. Enomoto, S. Furukawa, K. Fujita, Catalysts 11 (2021), 1200. https://doi.org/10.3390/catal11101200
6. S.B. Wadavrao, R.S. Ghogare, A.V. Narsaiah, Org. Commun. 6 (2013) 23–30.
7. A.A. Abu-Hashem, Am. J. Org. Chem. 5 (2015) 14–56. DOI: 10.5923/j.ajoc.20150501.03
8. P. Shanmugam, B. Viswambharan, S. Madhavan, Org. Lett. 9 (2007), 4095–4098. https://doi.org/10.1021/ol701533d
9. H.P. Deng, Y. Wei, M. Shi, Org. Lett. 13 (2011), 3348–3351. https://doi.org/10.1021/ol201094f
10. S.M. Anil, R. Shobith, K.R. Kiran, T.R. Swaroop, N. Malleshab, M.P. Sadashiva, New J. Chem. 43 (2019), 182–187 . DOI: 10.1039/C8NJ04936J
11. B. Karami, S. Khodabakhshi, J. Chil. Chem. Soc. 58 (2013) 1655–1658.http://dx.doi.org/10.4067/S0717-97072013000200002
12. P. T. Anastas and J. C. Warner, Green Chemistry: Theory and Practice, Oxford, New York (1998). https://doi.org/10.1093/oso/9780198506980.001.0001
13. P. T. Anastas and T. Williamson, Green Chemistry, Frontiers in Benign Chemical Synthesis and Procedures, Oxford (1998).

14. A. K. Nezhad, A. Zare, A.Parhami, A. Hasaninejad, A.R. Moosavi Zare, J. Iran. Chem. Soc. 5 (2008), 40-52. https://doi.org/10.1007/BF03245996
15. B. Ganley, G. Chowdhury, J. Bhansali, J. S. Daniels and K. S. Gates, Bioorg. Med. Chem. 9 (2001), 2395-2401. https://doi.org/10.1016/S0968-0896(01)00163-8
16. D. Benitez, M. Cabrera, P. Hernández, L. Boiani, M. L. Lavaggi, R. Di Maio, G. Yaluff, E. Serna, S. Torres, M. E. Ferreira, N. Vera de Bilbao, E. Torres, S. Pérez-Silanes, B. Solano, E. Moreno, I. Aldana, A. López de Ceráin, H. Cerecetto, M. González and A. Monge, J. Med. Chem. 54 (2011), 3624-3636. https://doi.org/10.1021/jm2002469
17. G. Aguirre, H. Cerecetto, R. Di Maio, M. González, M. E. Alfaro, A. Jaso, B. Zarranz, M. A. Ortega, I. Aldana, A. Monge-Vega. Bioorg. Med. Chem. Lett. 14 (2004), 13835-3839. https://doi.org/10.1016/j.bmc.2004.07.003
18. H.M.A. El-Wahy, Tetrahedron 56 (2000), 897-907. https://doi.org/10.1016/S0040-4020(99)01072-8
19. P. Ramalingam, S. Ganapaty, B. Rao, Bioorg. Med. Chem. Lett. 20 (2010), 406 -408. https://doi.org/10.1016/j.bmcl.2009.10.026
20. A.S. Khosarkar, D.B. Shinde, Bioorg. Med. Chem. Let. 16 (2006), 6181-6184. https://doi.org/10.1016/j.bmcl.2006.09.040
21. B. Obot, N. O. Egbedi, Mater. Chem. Phys. 122 (2010), 325-328 https://doi.org/10.1016/j.matchemphys.2010.03.037
22. B. Karami, S. Khodabakhshi, J. Chil. Chem. Soc. 58 (2013), 1655-1658. http://dx.doi.org/10.4067/S0717-97072013000200002
23. V. Elumalai, J.H. Hansen, SynOpen 5 (2021), 43-48. DOI: 10.1055/s-0040-1706021
24. Y. Li, Q. Peng, S. Li, Y. Cai, B. Zhang, K. Sun, J. Ma, C. Yang, H. Hou, H. Su, K. Li, Chemical. 301 (2019), 127-139. https://doi.org/10.1016/j.snb.2019.127139
25. S. Sajjadifar, S. Miri, Int. J. Chemtech Res. 6 (2014), 5433-5440.

26. Y. Kaya, S. Kaya, A. Berisha, & A. Ercag, J. Mol. Struct. 1291 (2023), 135973. https://doi.org/10.1016/j.molstruc.2023.135973

27. A. Mishra, S. Singh, M. A. Quraishi, V. Srivastava, Org. Prep. Proced. Int. 51 (2019), 345-356. https://doi.org/10.1080/00304948.2019.1596469

28. D.N. Kanekar, S.S Dhanawade, A.B Jadhav, M. Ghadiyali, S. Chacko, R. M. Kamble, Monatsh. Chem. 153 (2022), 895-906. https://doi.org/10.1007/s00706-022-02974-0V

29. H. S. N Prasad, A. P. Ananda, T. N. Lohith, P. Prabhuprasad, H. S. Jayanth, N. B. Krishnamurthy, M. A. Sridhar, L. Mallesha, P. Mallu, J. Mol. Struct. 1247 (2022), 131333-131347. https://doi.org/10.1016/j.molstruc.2021.131333

30. V. Nagalakshmi, R. Nandhini, V. Brindha, B. S. Krishnamoorthy, K. Balasubramani, J. Organomet. Chem. 912 (2020), 121175-121182. https://doi.org/10.1016/j.jorganchem.2020.121175

31. B. S. Krishnamoorthy, A. Thakur, K. K. V. Chakrahari, S. K. Bose, P. Hamon, T. Roisnel, S. Kahlal, S. Ghosh, J. F. Halet, Inorg. Chem. 51 (2013), 10375-10383. https://doi.org/10.1007/s00214-013-1356-6

32. N. Arumugam, S.M. Soliman, V. Viswanathan, A.I. Almansour, R.S. Kumar, S.M. Mahalingam, B.S. Krishnamoorthy, N. Dege, P. Karuppiah, K. Perumal, J. of Mol. Struct. 1293 (2023), 136189-136197. https://doi.org/10.1016/j.molstruc.2023.136189

33. R. Nandhini, B. S. Krishnamoorthy, G. Venkatachalam, J. Organomet. Chem. 903 (2019), 120984-120981. https://doi.org/10.1016/j.jorganchem.2019.120984

34. V. Brindha, B. S. Krishnamoorthy, Biointerface. Res. Appl. Chem. 14 (2024), 73-84. https://doi.org/10.33263/BRIAC143.073

35. S. Gomathi, K. Kavitha, N. Savitha, A. Mohana, V. Brindha, B. S. Krishnamoorthy, Lett. Appl. Nano BioSci. 12 (2023), 1-14. https://doi.org/10.33263/LIANBS124.105

36. B. S. Krishnamoorthy, S. Kahlal, S. Ghosh J. F. Halet, Theor. Chem. Acc. 132 (2013), 1356-1364. https://doi.org/10.1007/s00214-013-1356-6

37. D. D. Perrin, W. L. F. Armarego, Purification of laboratory chemicals, 4th edn. Butterworths-Heinemann, London, (1996).

38. G. M.Sheldrick, Acta Cryst. 71 (2015), 3-8. https://doi.org/10.1107/S2053229614024218

39. M. Kalidasan, R. Nagarajaprakash, S. Forbes, Y. Mozharivskyj, K. M. Rao, ZAAC. 641 (2015), 715-723. https://doi.org/10.1002/zaac.201400491

40. R. G. Parr, R. A. Donnelly, M. Levy, W. E. Palke, J. Chem. Phys. 68 (1978), 3801-3807. 1063/1.436185. http://dx.doi.org/10.1063/1.436185

41. R. G. Parr, R. G. Pearson, J. Am. Chem. Soc. 105 (1983), 7512-7516. https://doi.org/10.1021/ja00364a005

42. R. G. Parr, P. K. Chattaraj, J. Am. Chem. Soc. 113 (1991), 1854-1855. https://doi.org/10.1021/ja00005a072.

43. A. I. Almansour, N. Arumugam, S. M. Soliman, B. S. Krishnamoorthy, J. F. Halet, R. Vishnu Priya, J. Suresh, D. M. Althamili, F. A. Alaizari, R. S. Kumar, J. Mol. Struct. 1237 (2021), 130396. https://doi.org/10.1016/j.molstruc.2021.130396

44. Z. Zhou, R.G. Parr, J. Am. Chem. Soc. 112 (1990), 5720–5724. https://doi.org/10.1021/ja00171a007

45. R.G. Pearson, Z.B. Maksic (Eds.), Theoretical Models of Chemical Bonding Part II, Springer, Berlin, (1990), 45.

46. J. Luo, Z.Q. Xue, W. M. Liu, J. L. Wu, Z. Q. Yang, J. Phys. Chem. A. 110 (2006), 12005-12009. https://doi.org/10.1021/jp063669m

47. P. Forzatti, Appl. Catal. A. (2001), 222-236. https://doi.org/10.1016/S0926-860X(01)00832-8

48. C. M. Marian, U. Wahlgren, Chem. Phys. Lett. 251 (1996), 357-364. https://doi.org/10.1016/0009-2614(95)01386-5

49. B. A. Hess, C. M. Marian, U. Wahlgren, O. Gropen, Chem. Phys. Lett. 251 (1996), 365-371. https://doi.org/10.1016/0009-2614(96)00119-4

50. A. Becke, Phys. Rev. A. 38 (1986), 3098-3100. https://doi.org/10.1103/PhysRevA.38.3098
51. F. Neese, Wiley Interdiscip. Rev. Comput. Mol. Sci. 2 (2012), 73-78. https://doi.org/10.1002/wcms.81
52. S. H. Vosko, L. Wilk, M. Nusair, Can. J. Phys. 58 (1980), 1200-1211. https://doi.org/10.1139/p80-159
53. A. D. Becke, J. Chem. Phys. 84 (1986), 4524-4529. https://doi.org/10.1063/1.450025
54. J. P Perdew, Phys. Rev. B. 33 (1986) 8822-8824. https://doi.org/10.1103/PhysRevA.38.3098
55. H. Berman, K. Henrick, H. Nakamura, Announcing the worldwide protein data bank, Nat. Struct. Mol. Biol. 10 (2003), 980-980.
56. V. Rajendran, K. Ponnuraj, J. Biomol. Struct. Dyn. (2023). https://doi.org/10.1080/07391102.2023.2259483
57. C. Nantasenamat, A. Worachartcheewan, S. Prachayasittikul, N.A. Isarankura, V. Prachayasittikul, Eur. J. Med. Chem. 69 (2013), 99-114. https://doi.org/10.1016/j.ejmech.2013.08.015
58. E. D. Portakal, Y. Kaya, E. Demirayak, E. K. Yeldir, I. Kaya, J. Coord. Chem. 75 (2022), 611-628. https://doi.org/10.1080/00958972.2022.2070485
59. E. D. Portakal, Y. Kaya, E. Demirayak, E. K. Yeldir, I. Kaya, Appl. Organomet. Chem. 35 (2021), 6265-6272. https://doi.org/10.1002/aoc.6265
60. A. Daina, O. Michielin, V. Zoete, Sci. Rep. 7 (2017), 1-13. https://doi.org/10.1038/srep42717
61. F. Ameen, P. Srinivasan, T. Selvankumar, S. K. Kannan, S. A. Nadhari, A. Almansob, T. Dawoud, M. Govarthanan, Bioorg. Chem. 88 (2019), 102970-102973. https://doi.org/10.1016/j.bioorg.2019.102970

62. M. J. Deviprasad, B. S. Hemanth, M. B. Shivaswamy, H. S. N. Prasad, S. Sumathi, R. Aswathy, M. A. Sangamesha, A. P. Ananda, H. S. Jayanth, T. N. Lohith, BioNanoScience 14 (2024), 1-16. https://doi.org/10.1007/s12668-024-01583-x